UNSTEADY MIXED CONVECTION FLOW FROM A SLENDER CYLINDER DUE TO IMPULSIVE CHANGE IN WALL VELOCITY AND TEMPERATURE

by

***P. M. PATIL*[1]* and *I. POP*[2]**

[1]Department of Mathematics, JSS's Banashankari Arts, Commerce and Shanti Kumar Gubbi Science College, Vidyagiri, Dharwad – 580 004, India; E-mail:pmpmath@gmail.com

[2]Faculty of Mathematics, University of Cluj, R-3400 CLUJ, CP 253, Romania.

An unsteady mixed convection flow of a viscous incompressible fluid over a non-permeable linear stretching vertical slender cylinder is considered to investigate the combined effects of buoyancy force and thermal diffusion. It is assumed that the slender cylinder is in line with the flow. The unsteadiness in the flow and temperature fields is caused due to the impulsive change in the wall velocity and wall temperature of linearly stretching vertical slender cylinder. The effect of surface curvature is also taken into account, particularly for the applications as wire and fiber drawing where exact predictions are expected. The governing boundary layer equations are transformed into a non-dimensional form by a group of non-similar transformations. The resulting system of coupled non-linear partial differential equations is solved by an implicit finite difference scheme in combination with the quasi-linearization technique. Numerical computations are performed to understand the physical situations of linear stretching surface for different values of parameters to display the velocity and temperature profiles graphically. The numerical results for the local skin-friction coefficient and local Nusselt number are also presented. Present results are compared with previously published work and are found to be in excellent agreement.

Keywords: *unsteady flow; mixed convection; slender cylinder; impulsive change; linearly stretching sheet.*

Introduction

The flow and heat transfer characteristics induced by a stretching surface in a Newtonian fluid is of great practical importance because it occurs in many manufacturing processes in the polymer industry such as a polymer fibre is extruded continuously from a die with a tacit assumption that the fibre is inextensible. The cooling of a long metallic wire in a bath (an electrolyte) is another physical situation belonging to this category. Glass blowing, continuous casting, and spinning of fibers also involve the flow due to stretching surface. During its manufacturing process a stretched sheet interacts with the ambient fluid thermally and mechanically. The thermal interaction is governed by the surface heat flux.

This surface heat flux can either be prescribed or it is the output of a process in which the surface temperature distribution has been prescribed. Heat transfer over a stretching porous sheet subjected to power law heat flux in presence of heat source is recently studied by Hitesh Kumar [1]. However, in real life situations one has to encounter the boundary layer flow over the non-linear stretching surface. For example, in a melt-spinning process, the extrudate is stretched into a filament while it is drawn from the die. Finally, this surface solidifies while it passes through effectively controlled cooling system in order to acquire the top- quality property of the final product.

Flow over a cylinder is generally considered as two-dimensional phenomena as the radius of the cylinder is large enough compared to the boundary layer thickness. In contrast, for a slender cylinder when the radius of the cylinder is same as the order of the boundary layer thickness, the flow is considered to be axisymmetric. In the axisymmetric flow, the governing equations consists of the transverse curvature term which is strong enough to induce the behavior of flow and temperature fields and correspondingly, the skin friction coefficient and heat transfer rates over the surface. The impact of transverse curvature is vital in many applications such as wire and fibre drawing wherein accurate prediction is expected and thick boundary layer can exist on slender or near slender bodies. Suction or injection (blowing) of a fluid through the stretching surface, as, for instance, in mass transfer cooling, can significantly change the flow field and, as a consequence, affects the heat transfer rate from the surface.

Mixed convection flows, or coupled forced and natural convection flows arise in many transport processes both in natural and engineering applications. Such processes occur when the effects of buoyancy forces in forced convection or the effects of forced flow in natural convection become much more significant. The interaction between flow and thermal fields due to stretching of a boundary has very important role in many practical engineering applications. Unsteady mixed convection flows do not necessarily allow similarity solutions in many physical situations. The nonsimilarity and unsteadiness in such flow problems may be due to the free stream velocity or due to the curvature of the body or due to the surface mass transfer or even possibly due to all these phenomenal effects. Since the mathematical difficulties involved in obtaining nonsimilar solutions for such problems, many researchers and scientists have confined their work either to steady nonsimilar flows or to unsteady semi similar or self similar flows [2-4].

Chen and Mucoglu [5] and Mucoglu and Chen [6] have examined the effects of mixed convection boundary layer flow over an impermeable vertical slender cylinder due to the thermal diffusion with prescribed wall temperature and heat flux conditions, respectively. They obtained the solution by using the local non-similarity method. Further, Bui and Cebeci [7], Lee et al. [8] Wang and Kleinstruver [9],

and more recently, Takhar et al. [10] have solved this problem using an implicit finite difference scheme. Heckel et al. [11] have discussed the variable temperature effects on the mixed convection flow over a vertical cylinder. Recently, Kumari and Nath [12] analyzed the effects of localized cooling/heating and suction/injection on the mixed convection boundary layer flow on a thin vertical cylinder. Ishak et al. [13] analyzed the effects of injection and suction on the steady mixed convection boundary layer flows over a vertical slender cylinder with a free stream velocity and a wall surface temperature proportional to the axial distance along the surface of the cylinder. Dai et al. [14] have studied the localized phenomena in a slender cylinder composed by an incompressible hyperelastic material subjected to axial tension. In this study, authors have constructed analytical solutions based on a three dimensional setting and use the analytical results to describe the key features observed in the experiments by others. All the above studies are dealt with steady flows. In many practical situations, the flow could be unsteady due to the velocity of the moving cylinder which varies with time or due to the free stream velocity which also varies with time. Roy and Anilkumar [15] have investigated the unsteady effects on mixed convection flow over a moving vertical slender cylinder with surface mass transfer. Consequently, Singh et al [16] have examined the unsteady effects on mixed convection boundary layer flow from a rotating vertical slender cylinder in an axial flow.

The aim of the present analysis is to obtain a non-similar solution of an unsteady mixed convection boundary layer flow with combined effects of transverse curvature and thermal diffusion over a linearly stretching vertical slender cylinder, where the slender cylinder wall velocity and wall temperature changes suddenly arbitrarily with time. The non-similar solutions of the transformed equations are obtained numerically by solving a set of coupled nonlinear partial differential equations using the method of quasi-linearization in combination with the implicit finite difference scheme [17].

Mathematical formulation

Consider the unsteady mixed convection boundary layer flow over a nonpermeable stretching vertical slender cylinder of radius R and uniform temperature of the ambient fluid T_∞. The physical model and coordinate system considered are shown in Fig.1, where the radial coordinate r is measured from the axis of the cylinder and the axial coordinate x is measured vertically upwards such as $x = 0$ corresponds to the leading edge. The radius of the slender cylinder is the same as the order of the boundary layer thickness. Hence, the flow is taken to be axisymmetric. At time $t > 0$, the velocity U_0 of the moving cylinder is suddenly changed to $U_w(t,x) = U_0(x/R)(1+\varepsilon_1)\varphi(\tau)$ and the wall temperature is suddenly changed to $T_w(x) = T_\infty + \Delta T\,(x/R)(1+\varepsilon_2)$, where ε_1 and ε_2 are constants, τ is the

dimensionless time and ΔT is the characteristic temperature. Thermo-physical properties of the fluid in the flow model are assumed to be constant except the density variations causing a body force term in momentum equation. Further, it is assumed that the velocity $U_w(x,t)$ of the stretching cylinder is proportional to the distance x from the leading edge and time t, while the temperature $T_w(x,t)$ of the surface of the cylinder depends on x. It is also assumed that The Boussinesq approximation is invoked for the fluid properties to relate density changes to temperature changes, and to couple in this way the temperature field to the flow field [17 - 18]. In view of these aforementioned assumptions, the equation of conservation of mass, momentum and energy governing the mixed convection boundary layer flow over a stretching vertical slender cylinder can be expressed as:

$$\frac{\partial}{\partial x}(r\,u) + \frac{\partial}{\partial r}(r\,v) = 0 \tag{1}$$

$$\frac{\partial u}{\partial t} + u\frac{\partial u}{\partial x} + v\frac{\partial u}{\partial r} = \frac{\nu}{r}\frac{\partial}{\partial r}\left(r\frac{\partial u}{\partial r}\right) + g\,\beta(T - T_\infty) \tag{2}$$

$$\frac{\partial T}{\partial t} + u\frac{\partial T}{\partial x} + v\frac{\partial T}{\partial r} = \frac{\nu}{r}\frac{\partial}{\partial r}\left(r\frac{\partial T}{\partial r}\right) \tag{3}$$

The initial conditions are:

$$u(x,r,0) = u_i(x,r), \quad v(x,r,0) = v_i(x,r), \quad T(x,r,0) = T_i(x,r) \tag{4}$$

and the physical boundary conditions for the problem are given by:

$$\begin{aligned} &u(x,R,t) = U_w(x,t) = u(t,R,x) = U_w(t,x) = U(x)(1+\varepsilon_1)\phi(\tau), \quad v(x,R,t) = 0, \\ &T(x,R,t) = T_w(x) = T_\infty + \Delta T\,(x/R)^m\,(1+\varepsilon_2) \quad \text{at} \quad r = R \\ &u(x,\infty,t) \to 0, \quad T(x,\infty,t) \to T_\infty \quad \text{as} \quad r \to \infty \end{aligned} \tag{5}$$

where $\phi(\tau) = 1 + \alpha\tau^2$ with $\alpha > 0$ for accelerating flow and $\alpha < 0$ for decelerating flow, respectively.

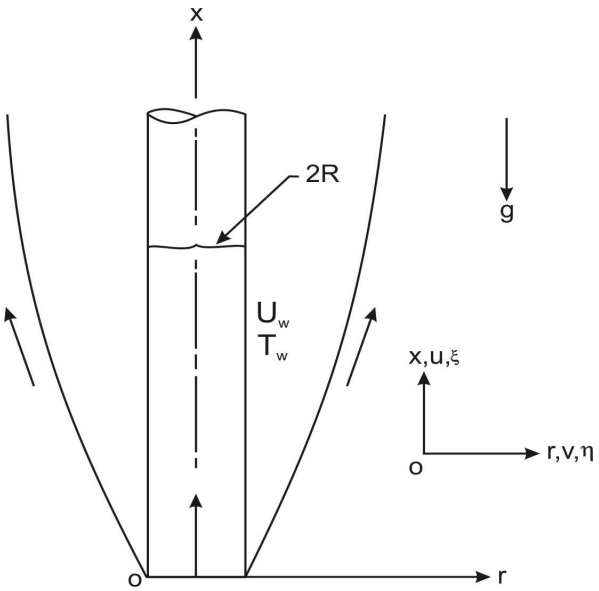

Fig. 1. Physical model and coordinate system.

Applying the transformations:

$$\xi = \left(\frac{4}{R}\right)\left(\frac{\nu x}{U(x)}\right)^{1/2}, \quad \eta = \left(\frac{U(x)}{\nu x}\right)^{1/2}\left(\frac{r^2 - R^2}{4R}\right), \quad \tau = \frac{\nu}{R^2}t$$
$$\psi(x,r,t) = R(\nu U(x)x)^{1/2}\,\phi(\tau)\,f(\xi,\eta,\tau), \quad G(\tau,\xi,\eta) = (T - T_\infty)/(\Delta T(x/R)^m) \tag{6}$$

where $U(x) = U_0(x/R)$ and ψ is the stream function, which is defined as $u = (1/r)\partial\psi/\partial r$ and $v = -(1/r)\partial\psi/\partial x$. We introduce also the notation $f_\eta(\xi,\eta,\tau) = F(\xi,\eta,\tau)$ where the index η denotes the partial differentiation with respect to η. Thus, we have

$$u = 2^{-1}U(x)\phi(\tau)F(\xi,\eta,\tau)$$
$$v = -\frac{R}{r}\left(\frac{\nu U(x)}{x}\right)^{1/2}\phi(\tau)\left[\left(\frac{m+1}{2}\right)f + \left(\frac{m-1}{2}\right)(\eta f_\eta - \xi f_\xi)\right] \tag{7}$$

Substituting (6) into Eqs. (2) and (3), we obtain the following transformed non-dimensional partial differential equations

$$\left[(1+\xi\eta)F_\eta\right]_\eta + 2\phi(\tau)\left[f F_\eta - F^2\right] + 8\phi(\tau)^{-1}(\tau)\lambda G - \left(\frac{\xi^2}{4}\right)\phi(\tau)^{-1}\left[\frac{d\phi(\tau)}{d\tau}F + \phi(\tau)\frac{\partial F}{\partial\tau}\right] = 0 \tag{8}$$

$$\left[(1+\xi\eta)G_\eta\right]_\eta + 2\,\mathrm{Pr}\,\phi(\tau)\left[f\,G_\eta - G\,F\right] - \mathrm{Pr}\left(\frac{\xi^2}{4}\right)\frac{\partial G}{\partial \tau} = 0 \tag{9}$$

The boundary conditions (5) become

$$\begin{aligned} &F(\xi,0,\tau) = 2\,(1+\varepsilon_1), \qquad G(\xi,0,\tau) = 1+\varepsilon_2 \quad \text{at} \quad \eta = 0 \\ &F(\xi,\infty,\tau) \to 0, \qquad\qquad G(\xi,\infty,\tau) \to 0 \qquad \text{as} \quad \eta \to \infty \end{aligned} \tag{10}$$

for $0 \le \tau,\, \xi \le 1$. Here $f(\xi,\eta,\tau) = \int_0^\eta F\,d\eta + f_w$ where $f_w = 0$ and λ is the constant mixed convection parameter, which is defined as

$$\lambda = \frac{Gr_x}{\mathrm{Re}_x^2} \tag{11}$$

where $Gr_x = g\,\beta\,\Delta T\,(x/R)\,x^3/\nu^2$ is the local Grashof number and $\mathrm{Re}_x = U_0\,(x/R)/\nu$ is the local Reynolds number. It is worth mentioning here that $T_w(x) > T_\infty$ refers to a heated cylinder (assisting flow) and $T_w(x) < T_\infty$ for a cooled cylinder (opposing flow), respectively. Therefore, the mixed convection (buoyancy) parameter $\lambda > 0$ indicates for assisting flow, $\lambda < 0$ for opposing flow and $\lambda = 0$ corresponds to forced convection flow. We have assumed that the flow is steady at time $\tau = 0$ and becomes unsteady for $\tau > 0$ due to the time dependent slender cylinder velocity $\left(U_w(x,t) = U(x)(1+\varepsilon_1)\phi(\tau)\right)$ and temperature $T_w(x,t) = T_\infty + \Delta T\,(x/R)(1+\varepsilon_2)$. Hence, the initial conditions (i.e. conditions at $\tau = 0$) are given by the steady state equations obtained from Eqs. (8) and (9) by substituting $\phi(\tau) = 1$, $d\phi/d\tau = \partial F/\partial\tau = \partial G/\partial\tau = 0$ when $\tau = 0$. The corresponding boundary conditions are obtained from (10). The main physical quantities of interest are the skin friction coefficient C_f and the local Nusselt number Nu_x, which represent the wall shear stress and the heat transfer rate at the surface of the cylinder, respectively. These coefficients are defined as

$$C_f = \frac{2\mu}{\rho U^2}\left(\frac{\partial u}{\partial r}\right)_{r=R}, \quad Nu_x = -\frac{x}{T_w(x) - T_\infty}\left(\frac{\partial T}{\partial r}\right)_{r=R} \tag{12}$$

where μ is the dynamic viscosity and ρ is the fluid density. Using (6) in (12), we obtain

$$\mathrm{Re}_x^{1/2}\,C_f = 2^{-1/2}\,\phi(\tau)\,F_\eta(\xi,0,\tau), \quad \mathrm{Re}_x^{-1/2}\,Nu_x = -2^{-1/2}\,G_\eta(\xi,0,\tau) \tag{13}$$

Numerical procedure

The non-linear coupled partial differential Eqs. (8) and (9) under the boundary conditions (10) have been solved numerically using an implicit finite difference scheme in combination with the quasi-

linearization technique [15, 16]. Quasi-linearization technique can be viewed as a generalization of the Newton-Raphson approximation technique in functional space. An iterative sequence of linear equations is carefully constructed to approximate the nonlinear Eqs. (8) and (9) under the boundary conditions (10) achieving quadratic convergence and monotonicity. With the help of quasi-linearization technique, the nonlinear coupled partial differential Eqs. (8) and (9) are replaced by the following sequence of linear partial differential equations.

$$F_{\eta\eta}^{\,i+1} + A_1^{\,i} F_\eta^{\,i+1} + A_2^{\,i} F^{i+1} + A_3^{\,i} F_\tau^{\,i+1} + A_4^{\,i} G^{i+1} = A_5^{\,i} \tag{14}$$

$$G_{\eta\eta}^{\,i+1} + B_1^{\,i} G_\eta^{\,i+1} + B_2^{\,i} G^{i+1} + B_3^{\,i} G_\tau^{\,i+1} + B_4^{\,i} F^{i+1} = B_5^{\,i} \tag{15}$$

The coefficient function with iterative index i are known and the function with iterative index (i+1) are to be determined. The corresponding boundary conditions of Eqs. (14) and (15) are given by

$$\begin{aligned} &F^{i+1}(\xi,0,\tau) = 2\,(1+\varepsilon_1), \quad G^{i+1}(\xi,0,\tau) = 1+\varepsilon_2 \qquad \text{at} \quad \eta = 0 \\ &F^{i+1}(\xi,\eta_\infty,\tau) = 0, \qquad\quad G^{i+1}(\xi,\eta_\infty,\tau) = 0 \qquad\quad \text{as} \quad \eta = \eta_\infty \end{aligned} \tag{16}$$

where η_∞ is the edge of the boundary layer. The coefficients in equations (14) and (15) are given by:

$$A_1^{\,i} = (1+\xi\eta)^{-1}\left[\xi + 2\phi(\tau)\, f\right]; A_2^{\,i} = -(1+\xi\eta)^{-1}\left[\frac{\xi^2}{4}\phi^{-1}(\tau)\frac{d\phi}{d\tau} + 4\phi(\tau)F\right]; \tag{17}$$

$$A_3^{\,i} = -(1+\xi\eta)^{-1}\frac{\xi^2}{4}; A_4^{\,i} = 8(1+\xi\eta)^{-1}\phi^{-1}(\tau)\lambda; A_5^{\,i} = -2(1+\xi\eta)^{-1}\phi(\tau)F^2;$$

$$B_1^{\,i} = (1+\xi\eta)^{-1}\left[\xi + 2\,\mathrm{Pr}\,\phi(\tau)F\right]; B_2^{\,i} = -2\,(1+\xi\eta)^{-1}\,\mathrm{Pr}\,\phi(\tau)F; B_3^{\,i} = -(1+\xi\eta)^{-1}\,\mathrm{Pr}\,\frac{\xi^2}{4}; \tag{18}$$

$$B_4^{\,i} = -2\,(1+\xi\eta)^{-1}\,\mathrm{Pr}\,\phi(\tau)G;\; B_5^{\,i} = B_4^{\,i} F\,.$$

Since the method is presented for partial differential equations in a recent study by Singh and Roy [16], its detailed description is not provided here. At each iteration step, the sequence of linear partial differential equations (14) and (15) were expressed in difference form using central difference scheme in the η- direction and backward difference scheme in ξ and τ directions. Thus in each step, the resulting equations were then reduced to a system of linear algebraic equations with a block tri-diagonal matrix, which is solved by Varga's algorithm [19]. To ensure the convergence of the numerical solution to the exact solution, step sizes $\Delta\eta$ and $\Delta\tau$ are optimized and taken as 0.005 and 0.01, respectively. The results presented here are independent of the step sizes at least up to the fourth decimal place. A convergence criterion based on the relative difference between the current and previous iteration values is employed. When the difference reaches 0.0001, the solution is assumed to have converged and the iteration process is terminated.

Results and Discussion

The computations have been carried out for various values of $\Pr(0.7 \le \Pr \le 7.0)$, λ $(-2.918 \le \lambda \le 10.0)$, ε_1 $(-0.5 \le \varepsilon \le 0.5)$, ε_2 $(-0.5 \le \varepsilon \le 0.5)$, τ $(0 \le \tau \le 1.0)$. The edge of the boundary layer (η_∞) has been taken between 2.0 and 5.0 depending on the values of the parameters. The results have been obtained for both accelerating $\left(\phi(\tau) = 1 + \alpha\tau^2; \alpha > 0, 0 \le \tau \le 1\right)$ and decelerating $\left(\phi(\tau) = 1 + \alpha\tau^2; \alpha < 0, 0 \le \tau \le 1\right)$ velocities of the fluid. The profiles drawn at $x = 0$ or $\xi = 0$ will represent the similarity solutions when all solutions along the $x-$ direction are made congruent using similarity transformations. In order to validate the accuracy of our method, we have verified our results with the steady state results of reduced skin friction and heat transfer coefficients $\left(f_{\eta\eta}(\xi,0), -G_\eta(\xi,0)\right)$ by direct comparison with the results previously reported by Chen and Mucoglu [5], Takhar et al. [10], and Roy and Anilkumar [15]. The comparisons are presented in Table 1 and are found to be in excellent agreement.

The effect of buoyancy parameter (λ) and Prandtl number ($\Pr$) on velocity and temperature profiles $\left(F(\xi,\eta,\tau), G(\xi,\eta,\tau)\right)$ for accelerating flow $\phi(\tau) = 1 + \alpha\tau^2, \alpha = 1$ with $\Pr = 0.7$ and $\xi = 0.5$ are displayed in Figs. 2 - 5. In buoyancy aiding flow $(\lambda > 0)$, the buoyancy force shows the overshoot in the velocity profiles $F(\xi,\eta,\tau)$ near the surface for fluids of lower Prandtl number (air, $\Pr = 0.7$) while for fluids of higher Prandtl number (water, $\Pr = 7.0$), the overshoot of the velocity is not much significantly observed as shown in Figs. 2 - 3. The magnitude of the velocity overshoot enhances with the buoyancy parameter $(\lambda > 0)$ while it reduces as Prandtl number increases (see Figs. 2 and 3). However, the influence of buoyancy force (λ) is larger for lower Prandtl number fluid (air, *Pr* = 0.7). The physical reason is that the lower viscosity of the fluid, which enhances the velocity profile within the stretching boundary layer as the assisting buoyancy force (λ) acts like a favorable pressure gradient. Thus, the velocity overshoot, occurs. For higher Prandtl number fluids (water, $\Pr = 7.0$), the overshoot is not significant because fluids with higher values of the Prandtl number implies more viscous fluid which have less impact on the buoyancy parameter (λ). It is very interesting to note from Fig. 2 that for opposing buoyancy flow, i.e. for negative values of the buoyancy parameter λ (< 0), the reverse

(back) flow occurs at $\lambda = \lambda_c \approx -0.295$, where λ_c (< 0) is the critical value of λ for which boundary layer separates from the cylinder.

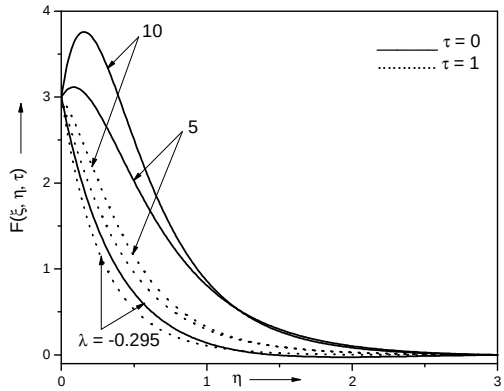

Figure 2: Effects of λ on velocity profile when Pr = 0.7 for $\phi(\tau) = 1 + \alpha\tau^2$, $\alpha = 1$, $\xi = 0.4$, $\varepsilon_1 = 0.5$, $\varepsilon_2 = 0.5$ and $m = 1$.

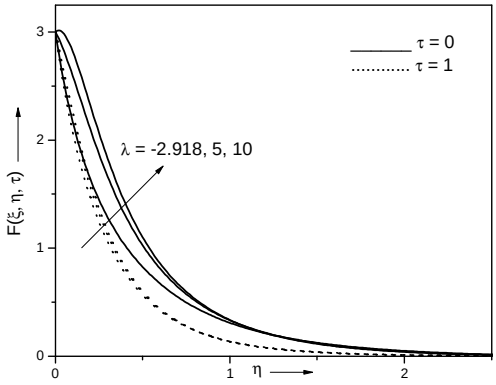

Figure: 3 Effects of λ on velocity profile when Pr = 7 for $\phi(\tau) = 1 + \alpha\tau^2$, $\alpha = 1$, $\xi = 0.4$, $\varepsilon_1 = 0.5$, $\varepsilon_2 = 0.5$ and $m = 1$.

It should be noticed that for $\lambda < \lambda_c$ (< 0), the boundary layer equations (12) and (13) have no solutions and the full Navier-Stokes and energy equations have to be solved. The buoyancy opposing force reduces the magnitude of the velocity considerably within the stretching boundary layer. The effect of time τ is crucial for the velocity overshoot. In particular, for $\alpha = 1$, $\Pr = 0.7, \varepsilon_1 = 0.5, \varepsilon_2 = 0.5$ and $\xi = 0.4$ at $\eta = 0.25$ when $\lambda = 10$, overshoot in the velocity profile reduced approximately by 43% as time τ increases from $\tau = 0$ to $\tau = 1$ when $m = 1$. The influence of buoyancy parameter (λ) has relatively less impact on the temperature profiles $G(\xi, \eta, \tau)$ and which are displayed here in Figs. 4 and 5. It is observed that the effect of $\Pr$ results into the thinner thermal boundary layer since the higher Prandtl number fluids (water, $\Pr = 7.0$) have lower thermal conductivity. Also, it is observed from Figs. 4 and 5 that the magnitude of the temperature profiles $G(\xi, \eta, \tau)$ decrease considerably within the thermal boundary layer when Pr = 7.0, i.e. for (water, $\Pr = 7.0$) as compared to Pr = 0.7 (air, *Pr* = 0.7).

Figures 6 - 7 display the skin friction coefficient and local Nusselt number $\left(\mathrm{Re}_x^{1/2} C_f, \mathrm{Re}_x^{-1/2} Nu_x\right)$ for accelerating and decelerating flows with $\phi(\tau) = 1 + \alpha\tau^2$, $\alpha = 1$ and $\alpha = -1$. We observe that the skin friction coefficient $\mathrm{Re}_x^{1/2} C_f$ decreases with the increase of buoyancy parameter (λ) (see Fig. 6).

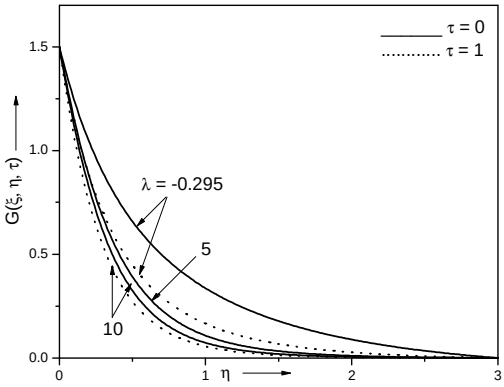

Figure 4: Effects of λ on temperature profile when Pr = 0.7 for $\phi(\tau) = 1 + \alpha\tau^2$, $\alpha = 1$, $\xi = 0.4$, $\varepsilon_1 = 0.5$, $\varepsilon_2 = 0.5$, Pr = 0.7 and $m = 1$.

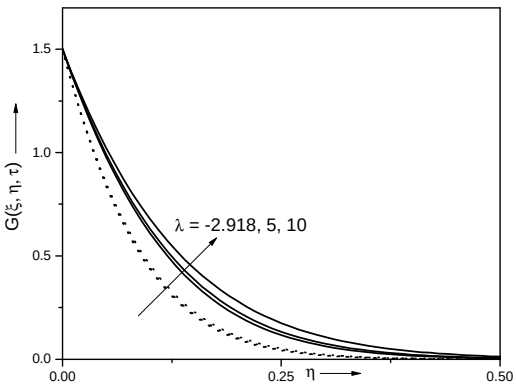

Figure 5: Effects of λ on temperature profile when Pr = 7 for $\phi(\tau) = 1 + \alpha\tau^2$, $\alpha = 1$, $\xi = 0.4$, $\varepsilon_1 = 0.5$, $\varepsilon_2 = 0.5$ and $m = 1$.

However, skin friction coefficient increases with the increase of Prandtl number from 0.7 to 7.0. The physical reason is that the assisting buoyancy force $(\lambda > 0)$ implies favorable pressure gradient, and the fluid gets accelerated, which results in thinner momentum and thermal boundary layers. For accelerating flows; for example, $\alpha = 1$, $\varepsilon_1 = 0.5$, $\varepsilon_2 = 0.5$ and $\xi = 1.0$ at $\tau = 0.5$, skin friction coefficient $\mathrm{Re}_x^{1/2} C_f$ decreases approximately about 62% and 6% as mixed convection parameter λ increases from 2.0 to 4.0 for $\mathrm{Pr} = 0.7$ and 7.0, respectively. In case of decelerating flows; for example, $\alpha = -1, \varepsilon_1 = 0.5$, $\varepsilon_2 = 0.5$ and $\xi = 1.0$ at $\tau = 0.5$, skin friction coefficient $\mathrm{Re}_x^{1/2} C_f$ decreases approximately about 20% and 83% , as λ increases from 2.0 to 4.0, respectively, for $\mathrm{Pr} = 0.7$ and 7.0, respectively. The behavior of skin friction coefficient $\mathrm{Re}_x^{1/2} C_f$ increasing monotonously with increasing time τ for accelerating flows while decreasing monotonously with increasing time τ in case of decelerating flows. Figure 7 describes the effects of mixed convection parameter λ and Prandtl number Pr on the local Nusselt number $\mathrm{Re}_x^{-1/2} Nu_x$. The local Nusselt number $\mathrm{Re}_x^{-1/2} Nu_x$ increases with increasing Pr as well as mixed convection parameter λ. In particular, for accelerating flows with $\alpha = 1, \varepsilon_1 = 0.5, \varepsilon_2 = 0.5$ and $\xi = 1.0$ at $\tau = 0.5$, due to the increase of mixed convection parameter increases from $\lambda = 2$ to $\lambda = 4$, the percentage increase of the local Nusselt number $\mathrm{Re}_x^{-1/2} Nu_x$ is approximately about 6% and just1% for Pr = 0.7 and 7.0 , respectively.

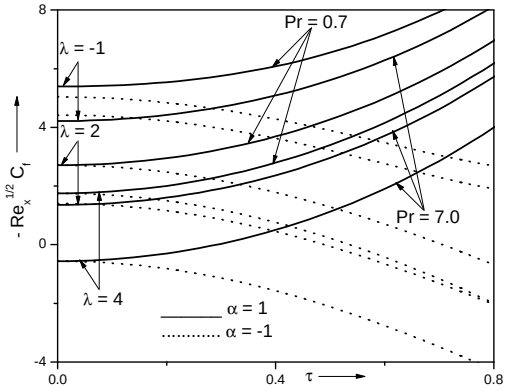

Figure 6: Effects of λ and Pr on skin friction coefficient for $\phi(\tau) = 1+ \alpha \tau^2$, ξ =1, ε_1= 0.5 and ε_2= 0.5.

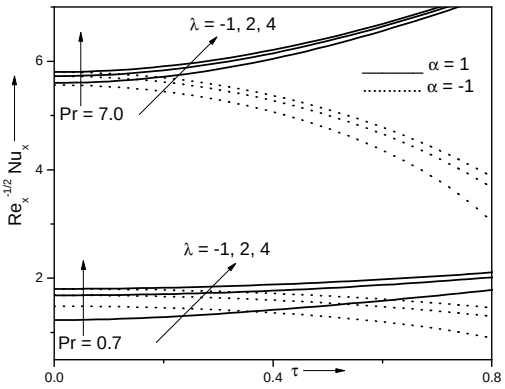

Figure 7: Effects of λ and Pr on heat transfer rate for $\phi(\tau) = 1+ \alpha \tau^2$, ξ =1, ε_1= 0.5 and ε_2= 0.5.

Similarly, for decelerating flows with $\alpha=-1, \varepsilon_1=0.5, \varepsilon_2=0.5$ and $\xi=1.0$ at $\tau=0.5,$ the percentage increase of the local Nusselt number $\mathrm{Re}_x^{-1/2}\, Nu_x$ is approximately about 123% and 120% at Prandtl number Pr = 0.7 and Pr = 7.0 respectively, when mixed convection parameter increases from $\lambda=2$ to $\lambda=4$. Further, it is noted that for accelerating flow ($\alpha=1$), local Nusselt number increases monotonously with increasing time τ while local Nusselt number $\mathrm{Re}_x^{-1/2}\, Nu_x$ decreases monotonously with increasing time τ for decelerating flow. The above characteristics in variation of local Nusselt number can also be followed from the temperature profiles presented in Figs. 3 and 4.

Figures 8 and 9 illustrate the role of wall velocity parameter ε_1 due to impulsive change and time τ on the velocity and temperature profiles $\left(F\left(\xi,\eta,\tau\right), G\left(\xi,\eta,\tau\right)\right)$ for accelerating flow $\phi\left(\tau\right)=1+\alpha\tau^2, \alpha=1,$ when $\lambda=2,\ \xi=0.5,\ \varepsilon_2=0.5$ and $\mathrm{Pr}=0.7$. The velocity and temperature profiles are influenced by the wall velocity parameter ε_1. In fact, velocity profile is decreasing with the wall velocity parameter ε_1 when it is suddenly reduced $\left(\varepsilon_1<0\right)$ i.e. $\varepsilon_1=0$ to - 0.5 while it is increasing as the wall velocity parameter ε_1 is suddenly increased $\left(\varepsilon_1>0\right)$ i.e. $\varepsilon_1=0$ to 0.5. However, the temperature profile is increasing with the wall velocity parameter ε_1 when it is suddenly reduced $\left(\varepsilon_1<0\right)$ while decreasing as wall velocity parameter ε_1 is suddenly increased $\left(\varepsilon_1>0\right)$. This clearly indicates that in an unsteady flow, an increase in the wall velocity parameter ε_1 acts as an accelerating force and hence fluid flow gets faster while decrease in the wall velocity parameter ε_1 acts as decelerating force and hence fluid flow gets slower.

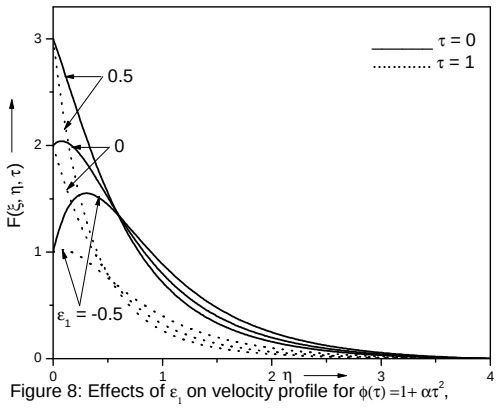

Figure 8: Effects of ε_1 on velocity profile for $\phi(\tau) = 1 + \alpha\tau^2$, $\alpha = 1$, $\xi = 0.5$, $\varepsilon_2 = 0.5$, $\lambda = 2$, Pr = 0.7 and $m = 1$.

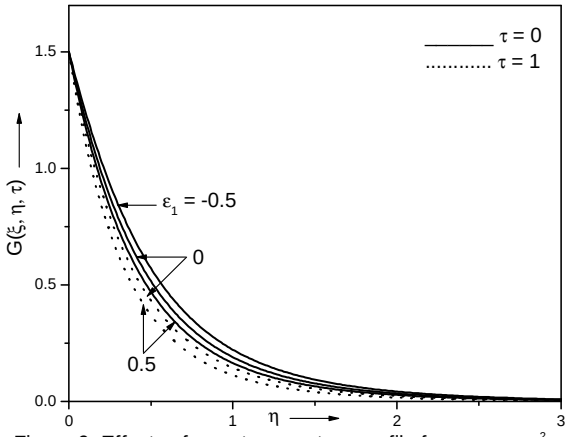

Figure 9: Effects of ε_1 on temperature profile for $\phi(\tau) = 1 + \alpha\tau^2$, $\alpha = 1$, $\xi = 0.5$, $\varepsilon_2 = 0.5$, $\lambda = 2$, Pr = 0.7 and $m = 1$.

The magnitude of the velocity and temperature profiles near the surface reduces with time τ. For example, $\alpha = 1, \lambda = 2, \xi = 0.5, \varepsilon_2 = 0.5,$ and $\Pr = 0.7$ at $\eta = 0.5,$ magnitude in the velocity and temperature profiles reduced approximately by 48% , 10% and 49% , 21% as τ increases from 0.0 to 1.0 at $\varepsilon_1 = -0.5$ and $\varepsilon_1 = 0.5$.

Figures 10 and 11 represent the influence of the wall velocity parameter ε_1 on the skin friction coefficient and heat transfer rate $\left(\mathrm{Re}_x^{1/2} C_f, \mathrm{Re}_x^{-1/2} Nu_x\right)$ when $\xi = 1, \ \lambda = 1, \varepsilon_2 = 0.5$ and $\Pr = 0.7$. Results indicate that the skin friction coefficient $\mathrm{Re}_x^{1/2} C_f$ and heat transfer rate $\mathrm{Re}_x^{-1/2} Nu_x$ increase with the increase of the wall velocity parameter ε_1. The wall velocity parameter ε_1 decreases from 0.5 to - 0.5, the skin friction coefficient $\mathrm{Re}_x^{1/2} C_f$ as well as the local Nusselt number $\mathrm{Re}_x^{-1/2} Nu_x$ decreases, as shown in Figs.10 and 11. In particular, for accelerating flows; for example, $\alpha = 1$, $\Pr = 0.7$, $\lambda = 1, \varepsilon_2 = 0.5$ and $\xi = 1$ at $\tau = 0.5$ the skin friction coefficient and heat transfer rate are to decrease approximately about 114% & 31%. Furthermore, for decelerating flows; for example, $\alpha = -1, \Pr = 0.7, \lambda = 1, \varepsilon_2 = 0.5$ and $\xi = 1$ at $\tau = 0.5,$ the skin friction coefficient and heat transfer rate decreases approximately about 220% and 29% as the wall velocity parameter ε_1 decreases from 0.5 to -0.5 at $m = 1$. Figures 12 and 13 depict the importance of the wall temperature ε_2 due to impulsive change and time τ on the velocity and temperature profiles $\left(F(\xi, \eta, \tau), G(\xi, \eta, \tau)\right)$ for

accelerating flow $\phi(\tau)=1+\alpha\tau^2, \alpha=1,$ when $\lambda=2,\ \xi=0.5,\ \varepsilon_1=0.5$ and $\Pr=0.7$. The velocity and temperature profiles are influenced by the wall temperature parameter ε_2.

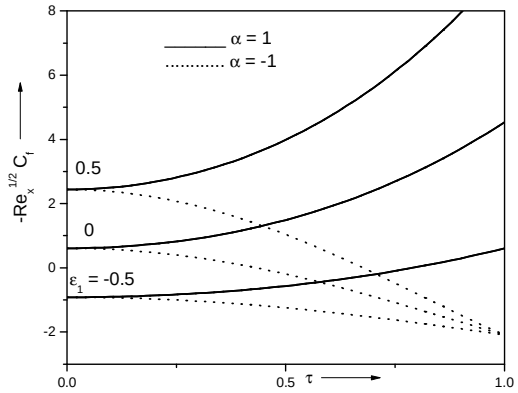

Figure 10: Effects of ε_1 on skin friction coefficient for $\phi(\tau) = 1+\alpha\tau^2$, $\xi=1$, $\lambda = 1$, Pr = 0.7 and $\varepsilon_2 = 0.5$.

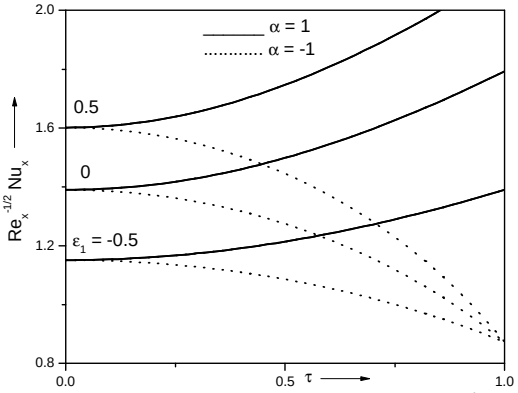

Figure 11: Effects of ε_1 on heat transfer rate for $\phi(\tau) = 1+\alpha\tau^2$, $\xi=1$, $\lambda = 1$, Pr = 0.7 and $\varepsilon_2 = 0.5$.

In fact, velocity and temperature profiles are decreasing with the wall temperature parameter ε_2 is suddenly reduced $(\varepsilon_2<0)$ i.e. $\varepsilon_2=0$ to - 0.5 while they are increasing as the wall temperature parameter ε_2 is suddenly increased $(\varepsilon_2>0)$ i.e. $\varepsilon_2=0$ to 0.5. This clearly indicates that in an unsteady flow, an increase in the wall temperature parameter ε_2 acts as an accelerating force and hence fluid flow and temperature gets enhanced while decrease in the wall temperature parameter ε_2 acts as decelerating force and hence fluid flow and temperature gets reduced. The magnitude of the velocity and temperature profiles near the surface reduces with time τ. For example, $\alpha=1, \lambda=2,\ \xi=0.5,\ \varepsilon_1=0.5,$ and $\Pr=0.7$ at $\eta=0.5$, magnitude in the velocity and temperature profiles reduced approximately by 45% , 24% and 49% , 21% as τ increases from 0.0 to 1.0 at $\varepsilon_2=-0.5$ and $\varepsilon_2=0.5$.

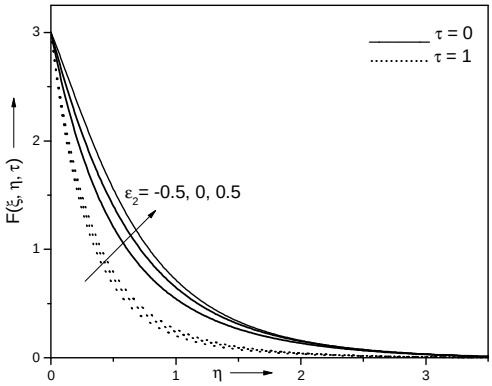

Figure 12: Effects of ε_2 on velocity profile for $\phi(\tau) = 1 + \alpha\tau^2$, $\alpha = 1$, $\xi = 0.5$, $\varepsilon_1 = 0.5$, $\lambda = 2$, Pr = 0.7 and $m = 1$.

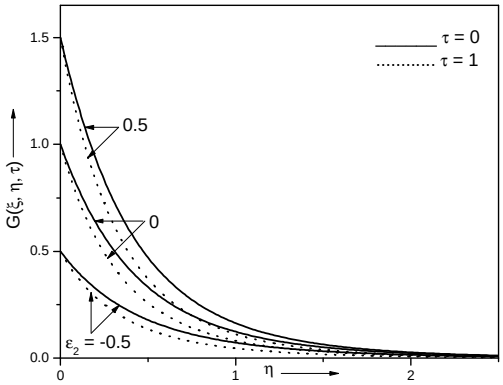

Figure 13: Effects of ε_2 on temperature profile for $\phi(\tau) = 1 + \alpha\tau^2$, $\alpha = 1$, $\xi = 0.5$, $\varepsilon_1 = 0.5$, $\lambda = 2$, Pr = 0.7 and $m = 1$.

Conclusions

A numerical investigation is performed to study an unsteady mixed convection flow over stretching vertical slender cylinder is considered to investigate the combined effects of buoyancy force and thermal diffusion, where the slender cylinder is in line with the flow. The unsteadiness in the flow and temperature fields is caused by the impulsive change in the wall velocity as well as in the wall temperature. Numerical results reveal that the buoyancy force (λ) and the Prandtl number (Pr) reduce the skin friction coefficient $\mathrm{Re}_x^{1/2} C_f$ and local Nusselt number $\mathrm{Re}_x^{-1/2} Nu_x$. The velocity profile exhibits significant enhancement for low Prandtl number fluid as compared to the magnitude of the velocity for higher Prandtl number. The velocity profile is enhanced due to sudden change in the wall velocity ε_1 while it is reduced when the wall velocity ε_1 is suddenly reduced. The velocity and temperature profiles are enhanced by wall temperature ε_2 suddenly changed while reduced due to sudden fall in the wall temperature.

Acknowledgements: Authors are thankful to the anonymous Reviewers for their useful detailed comments to improvise the paper. Dr. P M Patil dedicates this paper to one of his close friends **Shri B. L. Hosamani**, Assistant Commissioner of Commercial Taxes, Government of Karnataka, India who passed away very recently in road accident.

Nomenclature

C_f skin friction coefficient

C_p specific heat at constant pressure

f dimensionless stream function

F dimensionless velocity component

g acceleration due to gravity ($m\ s^{-2}$)

G dimensionless temperature

Gr_x $\left(g\,\beta_T\left(T_W\left(x\right)-T_\infty\right)x^3/\nu^2\right)$ local Grashof number

Nu_x local Nusselt number

Pr $\left(\nu/\alpha_m\right)$ Prandtl number

r radial coordinate (m)

R radius of cylinder (m)

Re_x $\left(U_\infty x/\nu\right)$ local Reynolds number

t dimensional time

T temperature

U_w stretching velocity of the cylinder ($m\ s^{-1}$)

u axial velocity component ($m\ s^{-1}$)

v radial velocity component ($m\ s^{-1}$)

x axial coordinate

Greek symbols

α unsteady parameter

α_m thermal diffusivity ($m^2\ s^{-1}$)

β volumetric coefficients of the thermal expansion (K^{-1})

τ dimensionless time

$\phi(\tau)$ unsteady function of τ

$\varepsilon_1, \varepsilon_2$ constants

ξ transverse curvature

η non-dimensional co-ordinate

λ $\left(Gr_x / \mathrm{Re}_x^{\,2}\right)$ buoyancy parameter (mixed convection) due to temperature gradient

μ dynamic viscosity ($kg.m^{-1}s^{-1}$, Pa.s)

ν $\left(\mu/\rho\right)$ kinematic viscosity ($m^2\ s^{-1}$)

ρ density ($kg.m^{-3}$)

ψ stream function

Subscripts

i initial condition

0 value at the wall for $\tau = 0$

w, ∞ conditions at the wall and infinity, respectively

x, r, t denote the partial derivatives with respect to these variables, respectively

ξ, η, τ denote the partial derivatives with respect to these variables, respectively

References

[1] Hitesh Kumar, Heat transfer over a stretching porous sheet subjected to power law heat flux in presence of heat source, Thermal Science (online), (2010), doi:10.2298/TSCI100331074K

[2] Anilkumar, D., Roy, S., Self-similar solution of the unsteady mixed convection flow in the stagnation point region of a rotating sphere, *Heat Mass Transfer*, 40 (2004), 6-7, pp. 487 – 493

[3] Roy, S., Anilkumar, D., Unsteady mixed convection from a rotating cone in a rotating fluid due to the combined effects of thermal and mass diffusion, *Int. J. Heat Mass Transfer*, 47 (2004), 8-9, pp.1673 – 1684

[4] Anilkumar, D., Roy, S., Unsteady mixed convection flow on a rotating cone in a rotating Fluid, *Applied Math. Comput.*, 155 (2004), 2, pp. 545 –561

[5] Chen, T. S., Mucoglu, A., Buoyancy effects on forced convection along a vertical Cylinder, *ASME J. Heat Transfer*, 97 (1975), 2, pp. 198 -203

[6] Mucoglu, A., Chen, T. S., Buoyancy effects on forced convection along a vertical cylinder with uniform heat flux, *ASME J. Heat Transfer*, 98 (1976), 3, pp. 523 -525

[7] Bui, M. N., Cebci, T., Combined free and forced convection on vertical slender cylinders, *ASME J. Heat Transfer*, 107 (1985), 2, pp. 476 – 478

[8] Lee, S. L., Chen, T. S., Armaly, E. F., Mixed convection along a vertical cylinders and needles with uniform surface heat flux, *ASME J. Heat Transfer*, 109 (1987), 3, pp. 711 -716

[9] Wang, T. Y., Kleinstruver, C., General analysis of steady mixed convection heat transfer on vertical slender cylinders, *ASME J. Heat Transfer*, 111(1989), 2, pp. 393 -398

[10] Takhar, H. S., Chamkha, A. J., Nath, G., Combined heat and mass transfer along a vertical moving cylinder with a free stream, *Heat Mass Transfer*, 36 (2000), 3, pp. 237-246

[11] Heckel, J. J., Chen, T. S., Armaly, B. F., Mixed convection along slender vertical cylinders with variable surface temperature, *Int. J. Heat Mass Transfer*, 32 (1989), 8, pp. 1431 – 1442

[12] Kumari, M., Nath, G., Mixed convection boundary layer flow over a thin vertical cylinder with localized injection/suction and cooling/heating, *Int. J. Heat Mass Transfer*, 47 (2004), 5, pp. 969 – 976

[13] Ishak, A., Nazar, R., Pop, I., The effects of transpiration on the boundary layer flow and heat transfer over a vertical slender cylinder, *Int. J. Non-linear Mech*, 42 (2007), 8, pp. 1010 – 1017

[14] Dai, H., Hao, Y., Chen, Z., On constructing the analytical solutions for localizations in a slender cylinder composed of an incompressible hyperelastic material, *Int. J. Solids Structures*, 45 (2008), 9, pp. 2613 – 2628

[15] Roy, S., Anilkumar, D., Unsteady mixed convection from a moving vertical slender Cylinder. *ASME J. Heat Transfer*, 128 (2006), 4, pp. 368 -373

[16] Singh, P. J., Roy, S. and Pop, I., Unsteady mixed convection from a rotating vertical slender cylinder in an axial flow, *Int. J. Heat Mass Transfer*, 51 (2008), 5-6, pp.1423 – 1430

[17] Schlichting, H., Boundary layer theory, Springer, New York, (2000)

[18] Pop, I., Ingham, D. B., Convective heat transfer: Mathematical and Computational Modelling of Viscous Fluids and Porous Media, Pergman, Oxford, (2001)

[19] Varga, R. S., Matrix Iterative Analysis, Prentice Hall, Englewood Cliffs, NJ. (2000)

Table 1. Comparison of the steady state results $\left(f_{\eta\eta}(\xi,0), -G_{\eta}(\xi,0)\right)$ with those of Chen and Mucoglu [5], Takhar et al. [10] and Roy and Anilkumar [15].

ξ	λ	Present results		Chen and Mucoglu [5]		Takhar et al. [10]		Roy and Anilkumar [15]	
		$f_{\eta\eta}(\xi,0)$	$-G_{\eta}(\xi,$	$f_{\eta\eta}(\xi,0)$	$-G_{\eta}(\xi,0)$	$f_{\eta\eta}(\xi,0)$	$-G_{\eta}(\xi,0)$	$f_{\eta\eta}(\xi,0)$	$-G_{\eta}(\xi,0)$
0	0	1.3283	0.5853	1.3282	0.5854	1.3281	0.5854	1.3282	0.5854
0	1	4.9666	0.8219	4.9666	0.8221	4.9663	0.8219	4.9664	0.8220
0	2	7.7124	0.9304	7.7126	0.9305	7.7119	0.9302	7.7122	0.9304
1	0	1.9171	0.8666	1.9172	0.8669	1.9167	0.8666	1.9169	0.8666
1	1	5.2584	1.0619	5.2584	1.0621	5.2578	1.0617	5.2580	1.0621
1	2	7.8874	1.1686	7.8871	1.1690	7.8863	1.1685	7.8871	1.1688